Bulletin of Mathematical Biology (2008) 70: 1684–1706
DOI 10.1007/s11538-008-9314-5

ORIGINAL ARTICLE

Stochastic Models for Phototaxis

Doron Levy[a,*], Tiago Requeijo[b]

[a] *Department of Mathematics and Center for Scientific Computation and Mathematical Modeling (CSCAMM), University of Maryland, College Park, MD 20742, USA*
[b] *Department of Mathematics, Stanford University, Stanford, CA 94305-2125, USA*

Received: 24 June 2007 / Accepted: 12 February 2008 / Published online: 22 July 2008

Abstract This work studies two mathematical models for describing the motion of phototactic bacteria, i.e., bacteria that move toward light. Based on experimental observations, we conjecture that the motion of the colony toward light depends on certain group dynamics. These group dynamics are hypothesized to be coordinated through an individual property of each bacterium, which we refer to as *excitation*. The excitation of each individual bacterium is assumed to change based on the excitation of the neighboring bacteria. Under these assumptions, we propose a (discrete) cellular automaton model and derive an analogous stochastic model for describing the evolution in time of the location of bacteria, the excitation of individual bacteria, and a surface memory effect. We provide simulation results and discuss in detail the role of the various model parameters in controlling the emerging dynamics.

Keywords Phototaxis · Cellular automaton · Interacting particles systems · Bacteria motion

1. Introduction

Bacteria have evolved sophisticated mechanisms in order to sense changes in environmental parameters such as light and nutrients. Under certain conditions, such changes will initiate a motion of an individual bacterium or of an entire colony in order to increase the resources availability. Bacteria that move toward light (to optimize conditions for photosynthesis) are called *phototactic*. The motion toward light is called *phototaxis*.

In this work, we are interested in studying the motion of a particular phototactic cyanobacterium, Synechocystis sp. Strain PCC6803. In a series of experiments reported in Burriesci and Bhaya (2008), time-lapse video microscopy was used to monitor the movement of individual cells and groups of cells. These movies suggest that in addition to the ability of single cells to move directionally, the overall time-evolution is determined by means of a group dynamics. Individual cells are less likely to move toward light while

*Corresponding author.
E-mail addresses: dlevy@math.umd.edu (Doron Levy), requeijo@math.stanford.edu (Tiago Requeijo).

cells that are grouped together are more likely to move. The observed dynamics appeared to be a complex function of cell density, surface properties, and genotype. Very little is known about the nature of the interactions between these parameters and its connection to phototaxis.

In recent years, the mathematical community has been showing a rapidly increasing interest in models of chemotaxis. At the same time, almost no attention has been devoted to modeling of phototaxis. Few examples include Childress et al. (1975) and Maree et al. (1999), none of which considers the group dynamics as a mechanism that is related to the motion. This paper and our previous works (Bhaya et al., 2008 and Levy and Requeijo, 2008) are the first attempts in that direction. Some of our preliminary results were announced in the conference proceedings (Bhaya et al., 2008). The more recent paper (Levy and Requeijo, 2008) was devoted to deriving a system of PDEs for describing phototaxis as the limit of a stochastically interacting many particle system. The system of PDEs resembled the Keller–Segel model for chemotaxis (Keller and Segel, 1971). It is derived following the ideas of Oelschläger (1989) and Stevens (2000b).

In this work, we derive and study mathematical models for describing the motion of phototaxis. To encode the observed group dynamics, we assume that every bacterium has an internal property, which we refer to as "excitation." The excitation of any bacterium is a time-dependent quantity that is adjusted based on the excitation of the neighboring bacteria. The excitation of a bacteria must exceed a predetermined critical threshold for it to initiate a motion in the direction of light.

Our first approach to the problem is based on a cellular automaton (CA). It is related to the CA model of Stevens (2000a) for chemotaxis. This CA takes into account the excitation of each bacterium and a surface memory effect. The qualitative behavior obtained when simulating this CA is very good as it captures the main characteristics of the phototaxis movement patterns. We then extend the CA model by introducing a stochastic model in which we track in time the locations of the individual bacterium, their excitation, and their trajectories in space. Numerical simulations of this stochastic model also show a qualitative behavior that is very similar to the observed experimental data. Most of this paper deals with discussing in detail the behavior and results obtained with both models.

The structure of this paper is as follows: In Section 3.1, we derive a cellular automaton which depends on the excitation and on a surface memory. The second model, the stochastic model, is presented in Section 3.2. The results from the numerical simulations are discussed in Section 4.1 for the cellular automaton, and in Section 4.2 for the stochastic model. Concluding remarks are given in Section 5.

2. Biological background

Burriesci and Bhaya (2008) used time-lapse video microscopy to track the movement of cells additional details about the motility are given in Bhaya et al. (2000). An analysis of the videos from Burriesci and Bhaya (2008) has led us to the following observations regarding the characteristics of the motion:

(1) *Delayed motion*. Even when the light is on, it will typically take a long time (minutes to hours) for a bacterium to initiate a motion toward the light source. When such motion develops, it is always observed in areas of a relatively high-density of bacteria. Individual bacterium will almost never initiate a motion toward light.

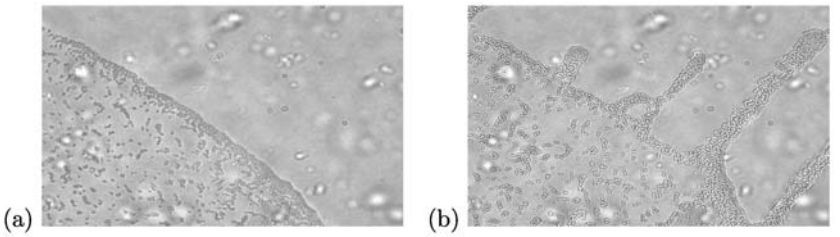

Fig. 1 Creation of fingers with a light source at the upper-right corner of the domain. Figure (a) shows the edge of the colony with single cells showing as dark dots. Figure (b) shows the fingers that are created from the areas of initial higher density.

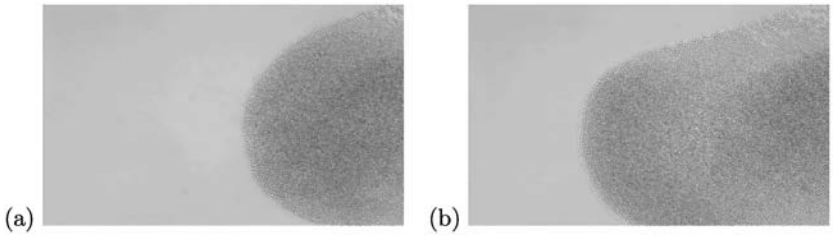

Fig. 2 Bacteria motion when the density is high. The snapshots were taken at increasing times. The light source is to the left of the domain.

(2) *Fingering*. In areas of low-density, bacteria tend to remain still or move slowly. When the density of bacteria is high, cells tend to move faster toward the light source. This "competition" between the inhomogeneously populated regions results with *fingers* such as those that are shown in Fig. 1. Bacteria that end up on the edges of these fingers seem to stop moving (or move very slowly). In some cases, it is even possible to observe *pinching*. This happens when the density of cells is high enough to form a finger, but as the finger is formed and bacteria move toward the light source, the density behind the leading tip decreases. Then if not enough bacteria is present, the tip eventually detaches. In all available movie sequences, the interfaces are very well defined; bacteria do not scatter to the outside of their own interface.

(3) *Density-dependent motion*. When the density of the cells is high, bacteria tend to move in one group toward the light (see Fig. 2). When the density of the cells is low and those cells are away from the interface edge, there is no clear preferred movement direction. Such a low-density motion is illustrated in Fig. 3.

(4) *Motion momentum*. Cells show a certain motion momentum: if they were in a lower density area (and hence moving slowly according to observation #2) they take time to start moving as fast as cells in other higher density areas. In Fig. 4, bacteria initially protrude from the front of the interface, but since the area is of low density, they move slowly for some time leading to the shape of the interface that is shown in snapshot (b).

(5) *A surface memory effect*. The movies suggest that when cells move, they mark the surface in a way that makes it more likely for other cells to revisit locations that were already traveled by other bacteria. The precise mechanism for the marking of

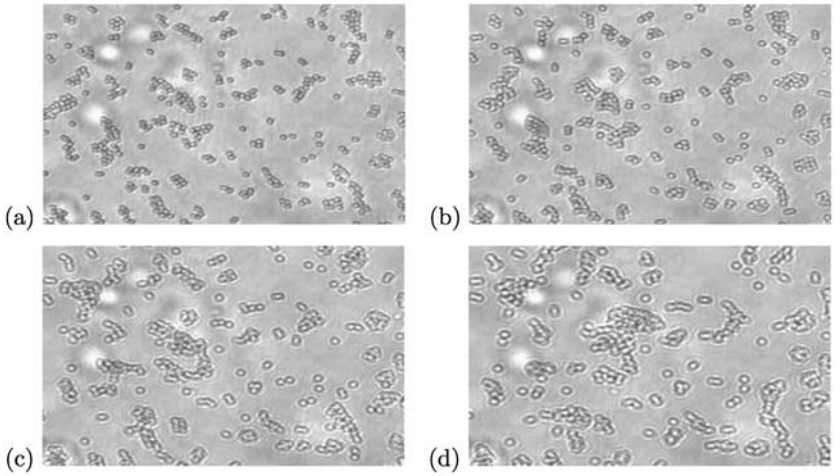

Fig. 3 A motion of bacteria when the density is low. There is no preferred direction for motion. The snapshots were taken at increasing times, starting from (a) and ending at (d). The light source is at the upper-right corner of the domain.

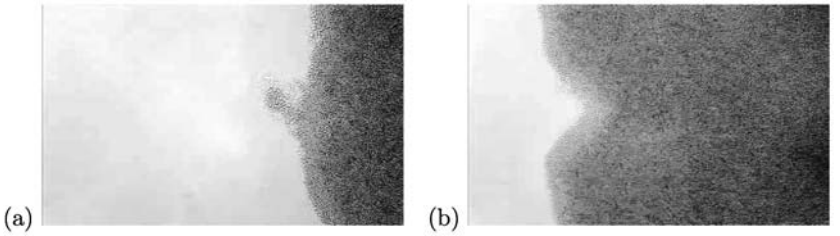

Fig. 4 Cells initially at the front of the domain move slower, and take some time to match the speed of faster cells (from higher density areas). The light is located to the left of the domain.

the surface with this particular strain of bacteria is unknown. There are other types of bacteria, such as Myxococcus Xanthus, for which a similar effect is known. In the case of Myxococcus Xanthus, a trail of polysaccharides is left behind by the moving bacteria, see e.g., Black et al. (2006), Li et al. (2003), Lu et al. (2005), Youderian and Hartzell (2006), Yu and Kaiser (2007). It is unknown whether a similar mechanism exists also with Synechocystis sp. Strain PCC6803, but the time-lapse movies suggest that this may be the case as indicated by the recent experimental study of Burriesci and Bhaya (2008). Another observation is that once a surface is traveled on, the corresponding surface memory does not seem to decay, at least not in the time scale we are interested in (hours). This issue has not been studied even for Myxococcus Xanthus, where such a long lasting effect could be generated, e.g., if bacteria do not consume the polysaccharides, or generate new polysaccharides instead of those that are consumed.

(6) *Sensing other bacteria*. Some movie sequences suggest that cells can sense other close-by cells even when they are not in contact with each other. An example is shown

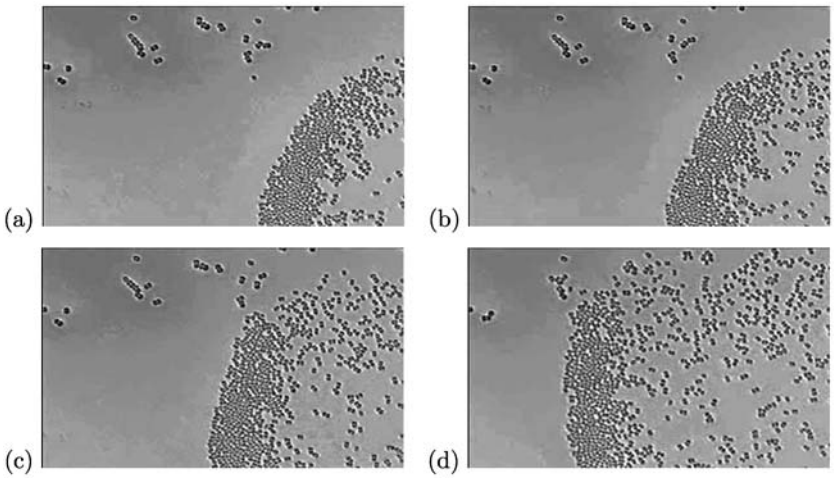

Fig. 5 The cells on the upper-left corner stay stationary before the cells from the back approach them. They then start moving before making any physical contact with the moving cells. The snapshots were taken at increasing times, starting from (a) and ending at (d). The light source is at the left side of the domain.

in Fig. 5. Cells that are located on the upper-left corner are stationary before the cells from the back get closer. However, they do start moving before they make any direct physical contact with the other cells.

2.1. Interpretation and assumptions

Based on the experimental results from Section 2, we draw some conclusions about some of the mechanisms that control phototaxis. The rest of this paper is based on the interpretation of experimental results and the assumptions mentioned here. We use the observations to construct a model that is based on the following three assumptions:

1. **Communication and excitation.** Observations #2 and #6, lead us to believe there exists some form of communication between bacteria. The mechanism proposed to describe such communication among cells is the existence of an *excitation* level that is associated with each cell. This excitation level is assumed to be closely related to the phototaxis phenomenon. Cells move toward the light whenever the excitation rises above a critical threshold (which we will refer to as the *excitation threshold*). The excitation associated with a given cell depends on the excitation of the surrounding bacteria. That is, cells propagate their excitation level to neighboring cells. The obvious expected results from such a mechanism include delayed motion (observation #1), motion momentum (observation #4), and a high-density motion as in observation #3. Delayed motion is a consequence of the time in takes cells to build up the excitation that is required to initiate a motion. For the same reason, this mechanism also implies motion momentum as cells take time to react to external configuration changes until their excitation mimics the excitation of surrounding cells. The motion pattern in

dense areas is a direct result of assuming that the excitation depends on the number of surrounding cells.

2. **Surface memory.** The second basic mechanism we base our model on is the surface memory effect (observation #5). Cells mark the surface (possibly with some substance they produce) in a way that facilitates the motion of other cells. This surface marking should also influence cells in a way that they are more likely to revisit previously occupied locations. An expected consequence of such a surface memory effect is a system with fairly well-defined interfaces. In addition to a preferable motion toward previously occupied locations, cells also tend to move faster on such areas. It is unknown (on the biophysical level) why cells that reach areas that were traveled on tend to accelerate their motion, but this is what is experimentally observed (Burriesci and Bhaya, 2008).
3. **Slow diffusion of cells.** Our third model assumption is that cells diffuse slowly. Such diffusion would then explain the low-density motion described in observation #3. One has to be careful in defining this diffusion effect, and balancing it against the surface memory effect: a large diffusion coefficient (when compared to the effects from the surface memory) will do away with the desired well-defined interfaces.

The dynamic finger formation (observation #2) is not a priori encoded into the model. It is possible to argue that this is a consequence of both the excitation and surface memory effect mechanisms. In inhomogeneously populated regions, cells build up excitation at different rates. This causes small clusters of cells to move toward the light source, while others stay behind. When those clusters move, they mark the surface behind them, making it easier for other cells with lower level of excitation to follow them, and consequently forming a finger (similar to the one shown in Fig. 1). The success of the mathematical models will be later assessed by their ability to reproduce the fingering patterns. We do not claim that our model assumptions are required for generating the fingers. Rather, we will show that models which are constructed following these assumptions, are capable of reproducing observations that were not directly taken into account when constructing the models.

As part of the model assumptions, we assumed that cells can communicate with each other. Indeed, it has been recently shown that in Synechocystis sp. there are rapid changes in cAMP levels that are triggered by light signals (Masuda and Ono, 2004, 2005; Ohmori and Okamoto, 1979). For example, an inactivation of adenylyl cyclase (*cya1*) or the CAP (*sycrp1*) resulted in a partially nonmotile phenotype (Bhaya et al., 2001; Terauchi and Ohmori, 1999; Yoshimura et al., 2002a, 2002b). However, the addition of cAMP can rescue this phenotype suggesting that cAMP plays a critical role in phototaxis. While cAMP is one of the known methods in which bacteria can "communicate" among themselves, the precise role of cAMP in phototaxis is yet to be investigated. Our models are not based on any explicit form of a communication between bacteria.

3. Models

In this section, we introduce models for the motion of phototactic bacteria that incorporate our assumptions about the mechanisms that control phototaxis. Numerical simulations of these models are provided in Section 4.

The first model we propose is a cellular automaton model in which time is discrete and cells move on a lattice in $\mathbb{R}^2$. Cellular automata are simple to implement, which makes them attractive for practical purposes. The cellular automaton model we propose includes a complex mechanism for encoding group dynamics.

We then proceed in Section 3.2 to formulate a continuous stochastic model that can be viewed as an extension of the cellular automaton model. In the stochastic model, we track in time the locations of the individual bacteria, their excitation levels, and their trajectories in space. Most of the simulations shown in Section 4 are of this stochastic phototaxis model.

The concluding comments of the section mention also a system of PDEs that can be obtained as the limit dynamics of a particle analog of the stochastic model from Section 3.2. A detailed derivation of the PDE model can be found in Levy and Requeijo (2008).

3.1. A cellular automaton model

In this section, we formulate a cellular automaton (CA) model. We assume a Cartesian grid of cells in $\mathbb{R}^2$ with a finite number of states. Time is taken to be discrete, and the state of a cell at time t depends on the automaton state at earlier times $s < t$. In each time step, bacteria are allowed to move to any of their eight nearest neighbors provided that they are not occupied. Additionally, we assume that the size of the bacteria population does not change in time.

Let $S_i(t) \in \mathbb{R}^+$ denote the excitation associated to bacterium i at time t. We assume that bacteria can sense the excitation of the surrounding bacteria and adjust their own excitation accordingly. We assume that the excitation of an individual bacterium will trigger a motion toward the light only if it is large enough. Accordingly, we introduce a critical threshold K. As long as $S_i(t) \leq K$, we say that bacterium i is not "sufficiently excited" to move toward the light.

To simplify the formulation, we assume that bacteria sense the light source from the left side of the domain. The rules of motion are the following:

R1. If the excitation $S_i(t)$ of cell i is below the critical level K, then the cell moves due to the surface memory effect with a given probability, or it diffuses with a very low probability if it did not move due to the surface memory effect.
R2. Otherwise, the cell moves mainly because of the excitation effect. The preferred motion is to the left, and it occurs when the neighboring cells on the left were previously occupied. If the immediate cell on the left is occupied, and if its diagonal neighbors to the left were previously occupied, the bacterium travels to one of these two locations with high probability.
R3. If the neighbors on the left were never occupied, we still follow the same rules of motion, but with lower probabilities.
R4. Finally, if the cell did not move due to the excitation effect, then it behaves just as if its excitation is below the critical level K, i.e., it moves due to the surface memory effect or it just diffuses with a very low probability.

These rules mean that the bacteria move preferentially toward the light, and the motion is facilitated on previously occupied cells. After computing the new positions for all bacteria, the excitation of every cell is updated based on the level of excitation of their new neighbors. The newly occupied locations are added to a matrix that represents all the

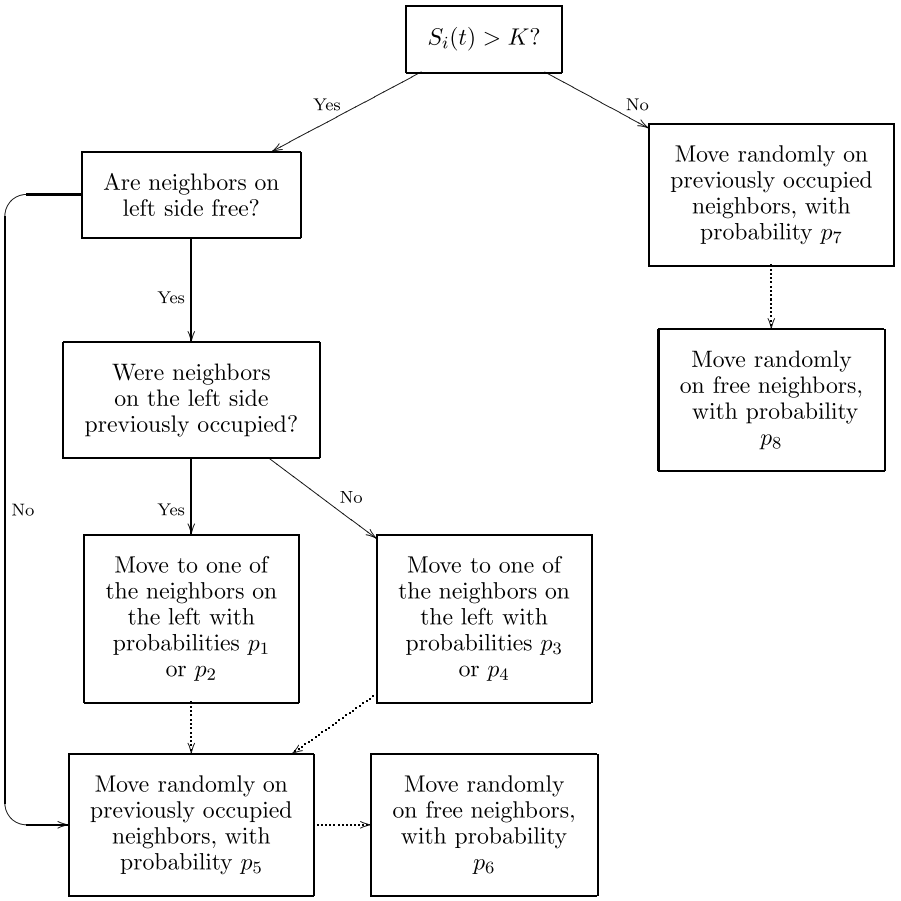

Fig. 6 The rules of motion for the cellular automaton model. The dotted lines are traversed only if the cell did not move in any of the previous steps. After applying these rules of motion to every cell in the colony, the excitation is updated based on the excitation of the new neighboring cells.

grid-cells that were traveled on starting from $t = 0$. The rules of the cellular automaton are summarized in Fig. 6.

3.2. A stochastic model

We now derive a continuous model that is based on the cellular automaton model from Section 3.1. We consider three different stochastic processes: the *position* of each bacterium at a given time, the *excitation* of each bacterium, and the *surface memory*.

We assume that the bacteria population is of a fixed size $N \in \mathbb{N}$ in $\mathbb{R}^2$, and denote the position of bacterium i at time $t \geq 0$ by $X_i(t) \in \mathbb{R}^2$. The excitation of the same bacterium is denoted by $S_i(t)$. The medium memory process will be denoted $L(t; x, y)$, with $(x, y) \in \mathbb{R}^2$.

In accordance with the observation made in Section 2.1, we assume that the surface memory effect does not diffuse as time evolves. We thus consider a stochastic process L that is given by the pure jump process

$$L(t; x, y) = \max_{\substack{0 \le s \le t \\ i=1,\ldots,N}} \delta_{(x,y)}\big(X_i(s)\big), \tag{1}$$

where $\delta_{(x,y)}$ is the Dirac delta function centered at (x, y) in $\mathbb{R}^2$. This definition means that the stochastic process L functions as a memory effect for the particle system, i.e., L keeps track of the paths of all bacteria.

Remark 3.1. It is possible to replace the jump process (1) by a continuous process. The representation (1) is convenient when it comes to the implementation as such an expression is then discretized. More details are provided in Section 4.

In order to describe the excitation process $S_i(t)$ for cell i, we let $\mu_i(t)$ denote the weighted average of the excitations of all cells contained in a small neighborhood of $X_i(t)$. This weighted average is given by

$$\mu_i(t) = \frac{1}{N} \sum_{j=1}^{N} \left[\left(1 - \frac{d(X_j(t), X_i(t))}{r} \right)^{+} S_j(t) \right], \tag{2}$$

where $d(\cdot, \cdot)$ is the Euclidean distance in $\mathbb{R}^2$. Note that $\mu_i(t)$ takes into account only neighboring bacteria that are within the domain of interaction. This domain is assumed to be a ball of fixed radius (r), which is identical for all bacteria. The quantity $\mu_i(t)$ thus provides a measure of the excitation in the neighborhood of bacterium i at time t.

For the excitation processes S_i, we assume a geometric mean-reverting process with a nonconstant mean-reverting level $\mu_i(t)$ of the form:

$$\frac{dS_i(t)}{S_i(t)} = \big(\mu_i(t) - S_i(t)\big)\, dt + \sigma\, dW_i(t). \tag{3}$$

The processes $W_i(t)$, $i = 1, \ldots, N$ are independent Wiener processes. The coefficient σ is assumed to be a quantity that is inherent to the given type of bacteria (and hence constant).

The definition (3) for the dynamics of $S_i(t)$ has the desirable consequence that the excitation of cell i follows the dynamics of the excitation of neighboring cells, but with some delay. That is, with $\mu_i(t)$ and $S_i(t)$ defined as above, we know that $S_i(t) > 0$ for all $t \ge 0$ and also that $S_i(t)$ tends to move toward the mean reverting level $\mu_i(t)$, which measures the excitation around cell i. We note that controlling $\mu_i(t)$ will implicitly control $S_i(t)$ (in particular, if μ_i is bounded, then the same will hold for S_i almost surely).

To define the position processes $X_i(t)$, we consider a light source that is located at infinity. The light is assumed to be always present and of uniform intensity. We also assume that all bacteria sense the light from the direction $\xi_t \in S^2$, where S^2 is the unit sphere in $\mathbb{R}^2$. The direction of light may depend on time, which is why we use the subscript t in ξ_t. To describe how bacteria react to the light and to the medium, we let $q: \mathbb{R}_0^+ \times \mathbb{R}_0^+ \times S^2 \to [0, 1]$ be a smooth function satisfying:

(1) q is strictly increasing in the first two variables.
(2) $\lim_{s\to\infty} q(s,\cdot,\cdot) = 1$.
(3) $q(0,\cdot,\cdot) = 0$.

We then define

$$dX_i(t) = v_s q\big(\big(S_i(t) - K\big)^+, L(t;x,y), L^\nabla(t;x,y)\big)\xi_t\,dt + v_g \nabla\rho^N(t;x,y)\,dt + v_r\,d\tilde{W}_i(t). \tag{4}$$

Here, $\tilde{W}_i(t)$ are independent 2-dimensional Wiener processes. The maximum velocity due to the excitation and the sensitivity to the surface memory is denoted by v_s, the maximum velocity due to the density gradient is denoted by v_g, and the maximum velocity due to the random phenomena is denoted by v_r.

The stochastic process ρ^N denotes the convolution of $\frac{1}{N}\sum_i \delta_{X_i}$ with a given mollifier φ^N that depends only on N. L^∇ is obtained from L by a fixed scaling of the gradient of $L * \varphi^N$, i.e.,

$$L^\nabla(x) = \frac{(L*\varphi^N)(x)}{1 + \|(L*\varphi^N)(x)\|}, \tag{5}$$

where $\|\cdot\|$ denotes the Euclidean norm in $\mathbb{R}^2$. Due to the scaling (5), L^∇ remains bounded, $\|L^\nabla(x)\| < 1$.

The model (1)–(4) accounts for sensitivity to the extra substance, sensitivity to light, natural group dynamics (not coming from reaction to light), and random phenomena. The natural group dynamics coming from $\nabla\rho^N(t;x,y)$ is a desirable effect, as observations seem to support that bacteria remain together even when there is no noticeable trend in movement. This translates into slow formation of cell aggregates in low density (when the density is large enough, cells get proportionally excited and start moving toward the light source after a time delay).

Remark 3.2. As mentioned above, we assume that the light source is always present. This assumption can be dropped by changing the processes $S_i(t)$ such that they rapidly decay when there is no light or by having them jump to values below the threshold K when the light is not present. It is also easy to extend the sensitivity function q so that it depends explicitly on $X_i(t)$, on the distance to the light source, and on the intensity of light.

Remark 3.3. In Levy and Requeijo (2008), we have derived a system of partial differential equations based on an interacting particle model that is the fully discrete analog of the model (1)–(4). In that setting, we wrote PDEs for the evolution in space and time of the densities of bacteria (u), total excitation (v) and the surface memory (l). The system we obtained in Levy and Requeijo (2008) was a system of reaction-diffusion equations with source terms that was of the form:

$$\begin{aligned}
\partial_t u &= \mu\Delta u - \nabla\cdot\big(g(v,u,l,\nabla l)u\big),\\
\partial_t v &= \mu\Delta v - \nabla\cdot\big(g(v,u,l,\nabla l)v\big) + \beta(u,v)u - \gamma(u,v)v,\\
\partial_t l &= \eta\Delta l + \lambda(u,l)u.
\end{aligned} \tag{6}$$

Here μ, and η are the diffusion coefficients. The function g is the sensitivity function that corresponds to the function q in (4). β and γ determine how excitation is produced (β) and depleted (γ), and λ regulates how quickly the surface memory is created. The main result of Levy and Requeijo (2008) is establishing the system (6) as the limit of a stochastically interacting particle system.

4. Numerical simulations

4.1. Simulations of the cellular automaton model

In this section, we present computational results that were obtained with the cellular automaton model from Section 3.1. In all simulations, a grid of size 400×150 was used. The algorithms to compute the state at time $(t+1)$ given the state at time t follow the automaton rules described in Section 3.1. All the random numbers needed in the simulations were drawn using the Mersenne twister random number generator.

For all simulations, we used the following values for the probabilities: $p_1 = 0.80$, $p_2 = 0.30$, $p_3 = 0.60$, $p_4 = 0.25$, $p_5 = p_7 = 0.30$, $p_6 = p_8 = 0.05$. At the end of each iteration, the excitation of each cell is updated in the following way: First, we decrease the excitation by a fixed percentage, q_1. We then add to its existing excitation a certain portion q_2 of the excitation of its four nearest neighbors. In our simulations, we used the values of $q_1 = 0.05$ and $q_2 = 0.015$.

The results shown in Figs. 7–9 demonstrate what can be obtained with such a model under three distinct initial configurations. In all examples, the light source is located to the left of the domain.

Example 1 (High-density). In the first example, the initial configuration has one high-density region of cells that is located at the right side of the domain. Snapshots of the time-evolution for this initial configuration are shown in Fig. 7. In this example, after an initial delay, the cells start moving. Due to the initial high density of the cells, the information regarding the excitation of individual cells can easily propagate to the neighboring cells. Hence, when the cells start moving, they move as a group and do not leave any cells behind.

Example 2 (Low-density). The second example is of an initial configuration with a low-density region of cells on the right side of the domain. Snapshots of the time-evolution for this configuration are shown in Fig. 8. In this case, most cells reach the required threshold to start moving toward the light source. A finger is created in an area where the initial density of cells was relatively high.

Example 3 (Surface memory). Our third CA example is shown in Fig. 9. In this case, we start with an initial configuration that contains several areas with a high-density areas of cells. We also mark an area on the right side of the domain as an area that was previously visited by bacteria (see Fig. 9(b)), even though it is initially vacant. This marking causes the two clusters of cells (above and below that area) to move toward each other (as shown in Fig. 9(c)). When excitation rises, cells start moving toward light as shown in Fig. 9(e).

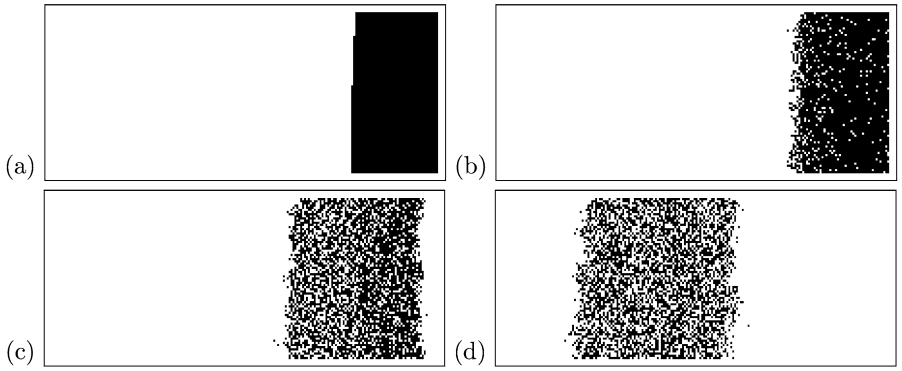

Fig. 7 Example 1. A cellular automaton simulation with a high-density initial configuration. The motion toward the light source (located to the left of the domain) starts after the excitation reaches the critical threshold. Since the excitation builds up in all cells, the entire population moves as a group without leaving any cells behind. Snapshots were taken at iterations 0, 60, 120, 300.

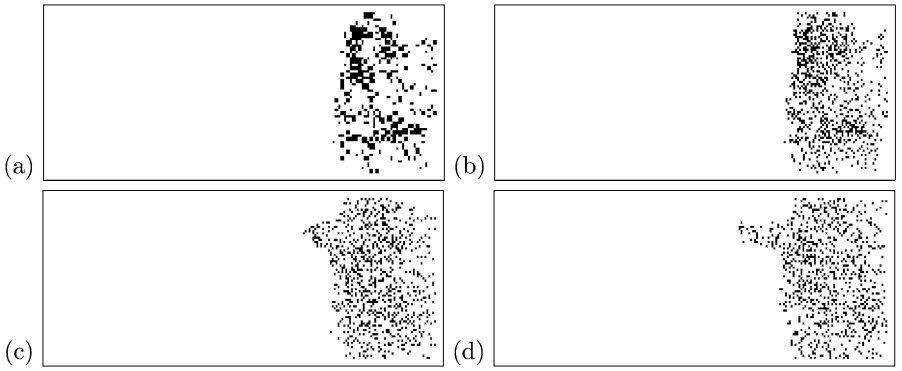

Fig. 8 Example 2. A cellular automaton simulation with a low-density initial configuration. The light source is located to the left of the domain. The excitation level in most cells never reaches the threshold required to initiate a motion toward the light source. A finger is being formed on the upper part of the domain (where the initial density was relatively high). The snapshots are taken at iterations 0, 50, 200, 500.

In all examples, it takes time to build up the required excitation that eventually triggers the motion toward light. In the mean time, the cells are subject to a stronger medium memory effect, and a weaker diffusion term. This causes them to follow paths that were previously occupied, without any particular directional tendency. This pattern of motion persists until their excitation reaches the threshold. Once the excitation passes the critical threshold, cells start moving rather quickly toward the light source.

4.2. Simulations of the stochastic model

In this section, we discuss results obtained from simulating the stochastic model from Section 3.2. For simplicity, the computations of the particle density ρ, the surface memory

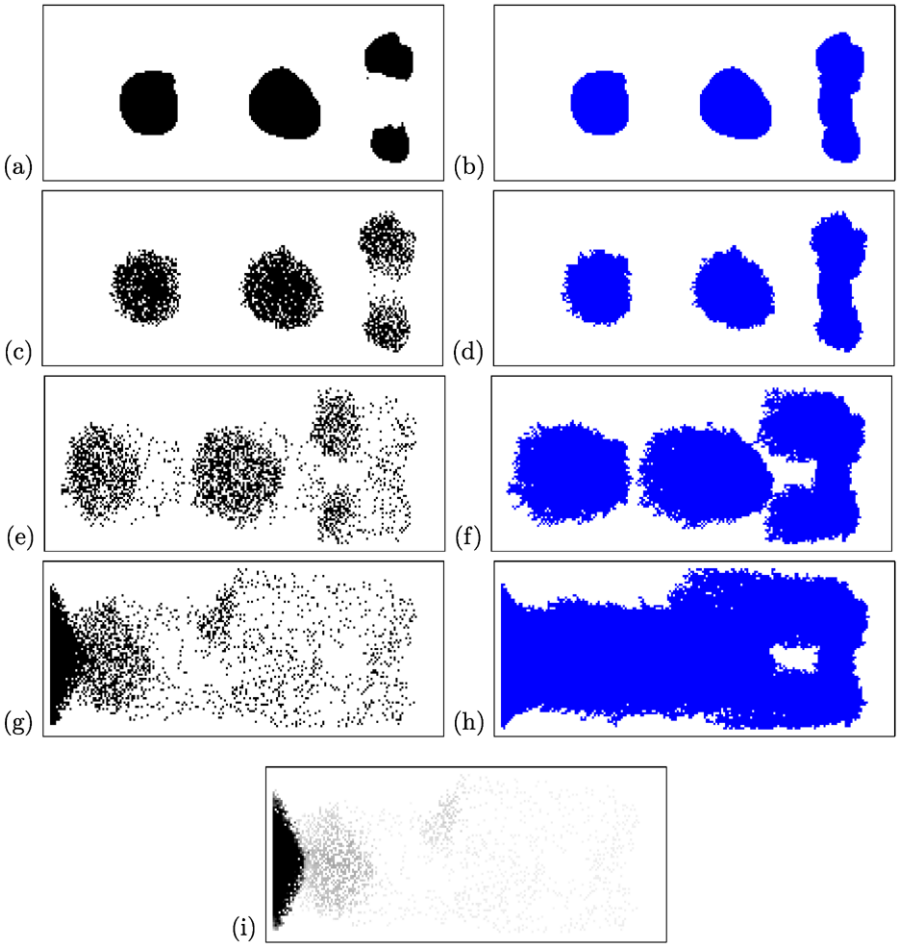

Fig. 9 Example 3. A cellular automaton simulation with an initial configuration that contains multiple high-density regions. The individual positions of the cells are shown on the left. The corresponding surface memory is shown on the right. The first four rows correspond to iterations 0, 60, 165, 365. Figure (i) shows the excitation on iteration 365 (higher excitation is darker). Note that the initial surface marking shown in figure (b) contains a marked surface that is vacant. This causes the (not yet excited) cells on the two clusters (above and below that region) to move toward each other (as shown in frame (c)). When the excitation rises, cells start moving toward the light as shown in (e). In (g), the higher density area on the top of the domain keeps moving closer to the previously occupied middle strip. Cells accumulate on the left side of the domain (frames (g)–(i)) since we do not allow them to exit.

effect L, and its gradient ∇L, were performed using an underlying Cartesian mesh with grid points that are spaced 0.05 units apart.

To localize the interactions, we assume that each bacterium can communicate only with neighboring bacteria that are located in a small neighborhood of the bacterium, which we refer to as the bacterium's *domain of interaction*. The domain of interaction is assumed

be identical for all bacteria, and is given by a ball of radius r that is centered at the individual bacterium.

Given the state at time t (i.e., the positions of all bacteria $X_i(t)$, the excitations of the bacteria $S_i(t)$, and the surface memory $L(t; x, y)$), we determine the state at the next time step, $t + \Delta t$, by updating (in this order), $S_i(t + \Delta t)$, $X_i(t + \Delta t)$, and $L(t + \Delta t, \cdot)$.

We use Euler's method to obtain $S_i(t + \Delta t)$ from $S_i(t)$, that is, we draw a random value $r_{\Delta t}$ from a normal distribution with mean 0 and variance Δt and set

$$S_i(t + \Delta t) = S_i(t) + S_i(t)\big(\mu_i(t) - S_i(t)\big)\Delta t + S_i(t)\sigma r_{\Delta t}.$$

The random numbers were drawn using a ziggurat algorithm that generates normally distributed random numbers from uniformly distributed numbers. The uniformly distributed numbers were drawn using the popular Mersenne twister random number generator.

The position process is updated in the same way as the excitation process. Euler's method is used to obtain $X_i(t + \Delta t)$ from $X_i(t)$. For the random term, two-dimensional normal values are drawn in the same way as the one-dimensional values. To compute $\nabla \rho^N$ we use the underlying Cartesian mesh to determine the density at each grid point, and approximate the gradient using finite differences. The densities only take into account the number of bacteria in the domain of interaction.

The computation for L^∇ is straightforward since we are only interested in its directional component pointing to the light source. Also, at the point (x, y) where a given bacterium currently is, it is always the case that $L(t; x, y) = 1$. Hence, the directional derivatives of L are zero if and only if a bacteria ever occupied the nearest directional neighbor. After computing the positions for time $t + \Delta t$, we update the function $L(t + \Delta t; x, y)$ by setting it to 1 at the points $X_i(t + \Delta t)$, $i = 1, \ldots, N$.

The sensitivity function q is assumed to be of the form

$$q(s, l, w) = \begin{cases} 1 - e^{-s}, & \text{if } w = 0, \\ \alpha_q(1 - e^{-s}), & \text{otherwise.} \end{cases} \tag{7}$$

Here, $\alpha_q \in (0, 1)$ is a constant representing the sensitivity to the medium (α_q close to 1 means that the medium offers almost no resistance to movement). The two different branches highlight how the medium memory effect enters into play: although bacteria still move when the excitation is above the threshold, they move α_q^{-1} times faster than if other bacteria previously occupied that point.

In all simulations, we set the directional light source vector as $\xi_t = (-1, 0)$, i.e., the light source is located to the left of the domain.

Remark 4.1. Note that our choice for q in (7) does not depend on l. This is because at the end of each iteration, we set $L(t + \Delta t; x, y) = 1$ at the points $X_i(t + \Delta t)$. Hence, we can assume $l = 1$ when choosing q.

We are now ready to present the simulation results that were obtained with various initial distributions of bacteria, and discuss the main characteristics of this model. Unless otherwise stated, the results refer to a population of 5,000 bacteria with an initial excitation $S_i(0)$ that are slightly above machine zero. The following parameters are used: $\Delta t = 0.1$, $\sigma = 0.3$, $r = 2$, $v_s = 1.5$, $v_b = 0.05$, $v_g = 0.01$, $K = 0.15$, and $\alpha_q = 0.2$.

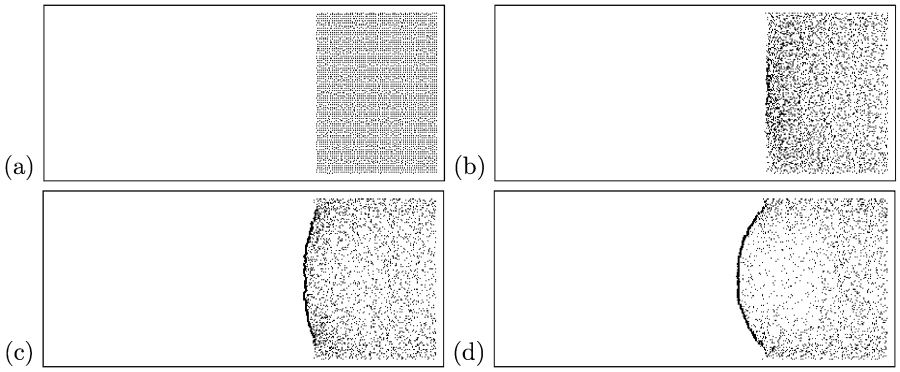

Fig. 10 Example 4. A simulation of the stochastic model with an initial high-density distribution of bacteria. The light source is located to the left of the domain. Shown are the positions of every bacteria. A moving front develops on the left. The snapshots taken refer to the initial setting (a), iteration 50 (b), iteration 100 (c), and iteration 150 (d).

Example 4 (Movement in high-density areas). In this simulation, we start with bacteria that are equally spaced in $\mathbb{R}^2$, forming a square of size 4×4 units. In the results that are shown in Fig. 10, we observe a pattern of motion that is similar to the experimental sequence shown in Fig. 2. Notice that the bacteria that are closer to the light source from a moving front. At the same time, the bacteria that are on the right side of the domain are left behind. The results of this simulation should be compared with the simulation of the CA model with a similar high-density initial data (shown in Fig. 7). For a similar initial configuration, the stochastic model does support a finger formation, which is not the case with the CA.

Example 5 (Delayed motion). To show that this model also captures the delayed motion effect discussed in Section 2.1, we start with 5,000 bacteria that are equally spaced in a rectangle of size 1×6. We also consider a higher threshold than before, $K = 0.4$, so that it is easier to observe the delay in initiating the motion. Due to the higher threshold level, bacteria require more time to build up their excitation in order to start moving toward the light source. Figure 11 shows a particular simulation with this setting. From (a) to (b), there is no clear movement trend. In (c), we start observing a displacement of some bacteria toward the left, but it is still not a very strong effect. This is because only for few bacteria the excitation exceeds the critical threshold. As these few bacteria propagate their excitations to neighboring bacteria, more cells start moving. The evolution from (c)–(d) shows that cells are moving toward the light source.

Example 6 (Finger creation). In this simulation, 5,000 bacteria are initially normally distributed in $\mathbb{R}^2$. The results are shown in Fig. 12. Bacteria closer to the center are in a higher density area and hence gain excitation faster. This translates into a faster movement toward the light source. As this motion progresses, bacteria that are left behind sense less particles and take longer to start moving. This results in the creation of a finger. Most of the bacteria are in the front of the domain, which eventually results in the tip detaching (not shown in the figure). This happens because there are not enough bacteria in the back

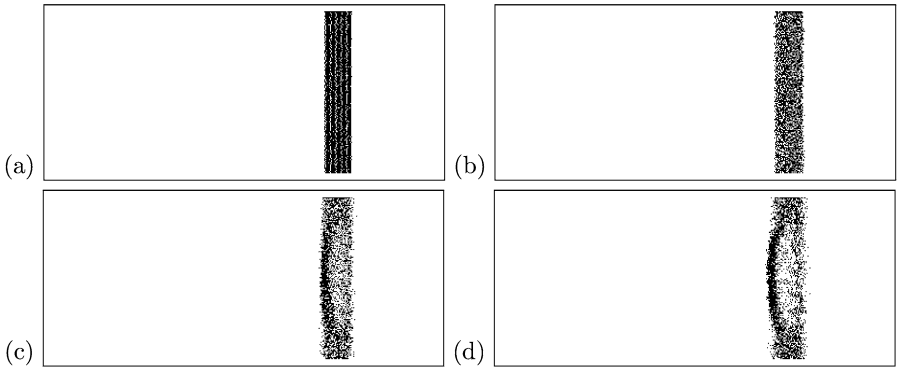

Fig. 11 Example 5. A simulation of the stochastic model with a large excitation threshold, $K = 0.4$. Due to the value of K, it takes more time for bacteria to build up the excitation that is required to start moving toward the light source. Shown are the positions of every bacteria initially (a), at iterations 50 (b), 200 (c), and 500 (d).

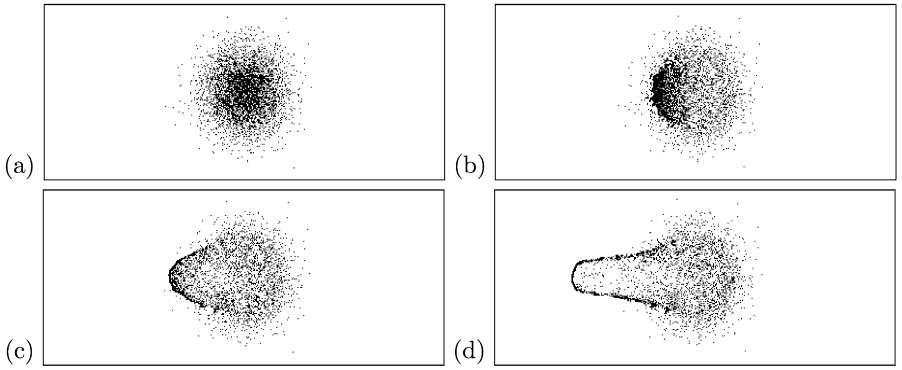

Fig. 12 Example 6. A simulation of the stochastic model showing a finger formation. Bacteria that are closer to the center are in areas of a relative higher density. Hence, their excitation increases faster. They move faster and a finger forms. Snapshots show the positions of bacteria, as taken at the initial setting (a), iteration 50 (b), iteration 100 (c), and iteration 200 (d).

of the domain to compensate for the excitation that is lost when faster (and more excited) bacteria move out of the domain of interaction of bacteria that are left in areas of low density. This pattern of motion is similar to the experimental results shown in Fig. 1.

Example 7 (Surface memory effect). To demonstrate the role that the surface memory effect plays, we divide the set of particles into two subsets of 2,500 bacteria. Each of those subsets is normally distributed in $\mathbb{R}^2$, with means $(0, 0)$ and $(5, 0)$ (see Fig. 13). Bacteria in both subsets initially have a similar movement pattern; they group in two fronts and start forming a finger. After some time, the finger on the right side of the domain reaches the location where bacteria on the left initially were at. When this happens, the right finger starts moving faster due to the surface memory effect: when bacteria arrive at locations

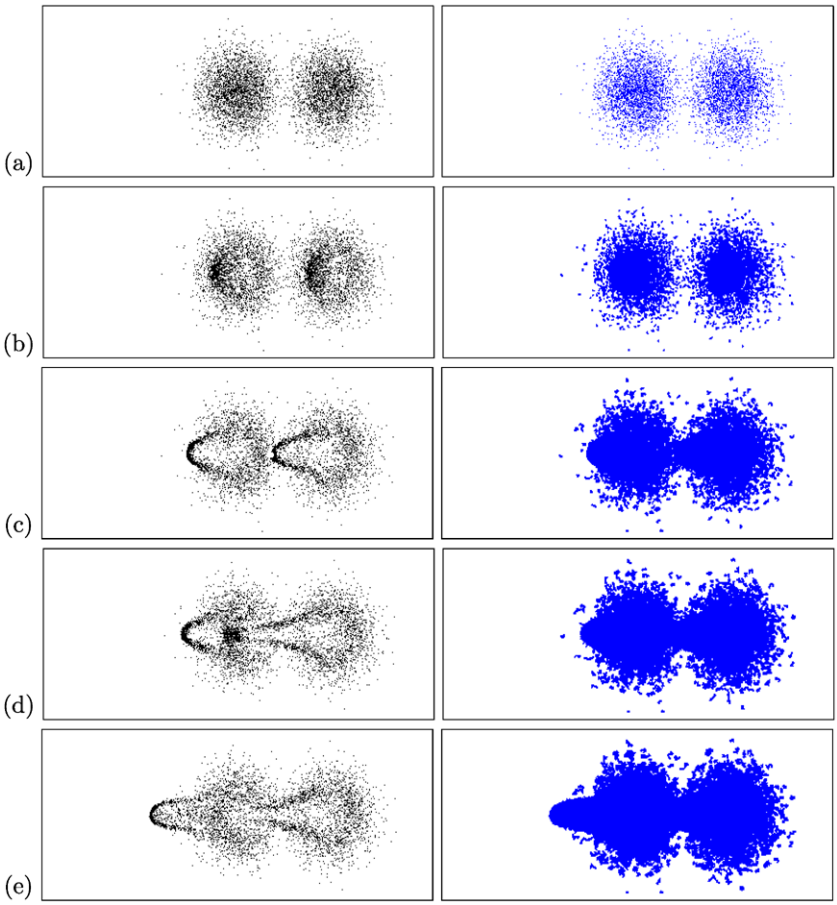

Fig. 13 Example 7. A simulation showing the role of the surface memory effect in the stochastic model. Initially, bacteria move at a somewhat uniform speed when they travel on areas that have not been previously occupied (a)–(b). At a later time, the bacteria belonging to the right finger reach locations that were previously occupied by other bacteria and increase their speed (c). They eventually catch up with the finger on the left (d)–(e). The positions are shown in the left column. The medium memory function L in shown in the right column. The snapshots correspond to iterations 0, 100, 400, 700, and 1200.

that were previously occupied, they can move substantially faster (as observed in the experiments of Burriesci and Bhaya, 2008). In this context, it is important to emphasize that the surface memory effect, as embedded in our model, is not only one of recognition, but also of speed: Once bacteria move into areas that were previously traveled by other bacteria, they accelerate their speed. The results are shown in Fig. 13.

Example 8 (Excitation effect). In this simulation, shown in Fig. 14, we start with a mixture of high-density and low-density areas. We start with 5,000 bacteria that are divided into two subsets, one containing about twice as many bacteria as the other. Each subset is normally distributed. Bacteria in the higher density area start moving toward the light,

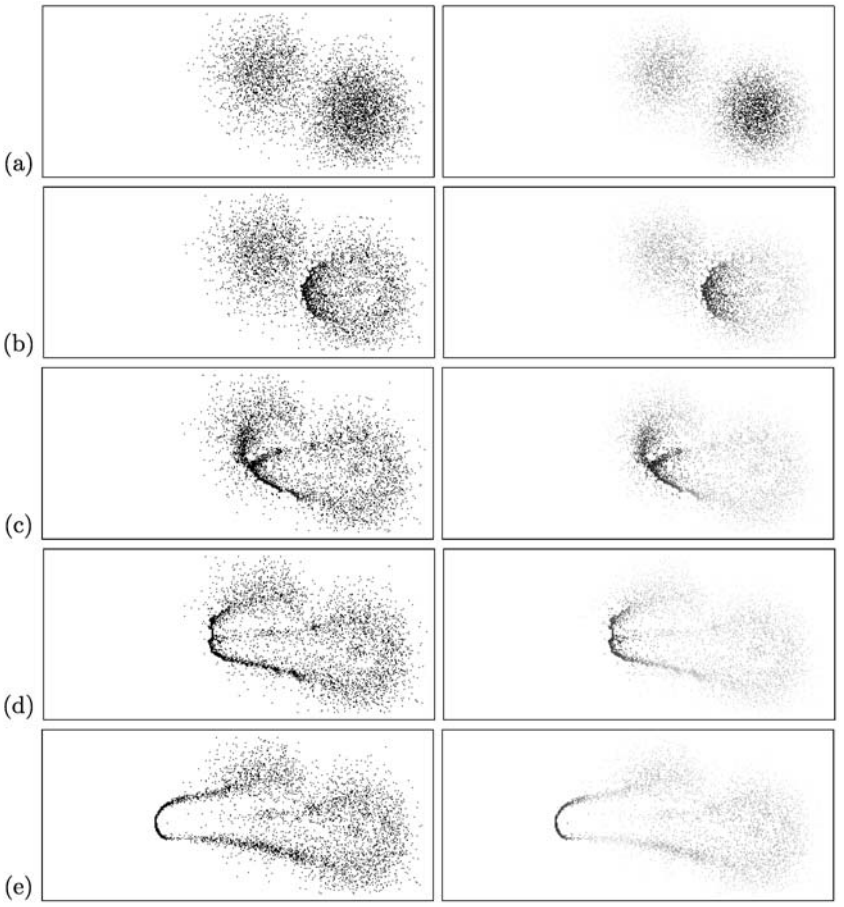

Fig. 14 Example 8. Simulation showing the propagation of excitation in the stochastic model. The positions of the bacteria are shown in the left column. The corresponding excitations are shown in the right column (darker areas correspond to a high excitation value). The snapshots taken refer to iterations 0, 100, 200, 300, and 600. Bacteria in the high-density region have an initial higher speed (b). In (c), bacteria in the low-density area, are already sensing the finger formed from the higher density area. It is clear that in (d), bacteria in the lower density area are highly excited and are pulled along with the finger (it is still possible to distinguish between the two different areas). At a later time (e), a thicker finger is formed from the two narrow fingers.

while the ones in lower density area almost do not move. When the fast bacteria get close enough to other bacteria, their high excitation level propagates to the neighboring bacteria, which then join the group and widen the finger. This is similar to the experiments shown in Fig. 5.

Example 9 (The effect of the medium sensitivity coefficient α_q). The medium sensitivity coefficient α_q in (7) determines how strongly the medium slows down bacteria. If a particular location $(x, y) \in \mathbb{R}^2$ was not occupied up to time t, bacteria moving to (x, y) will

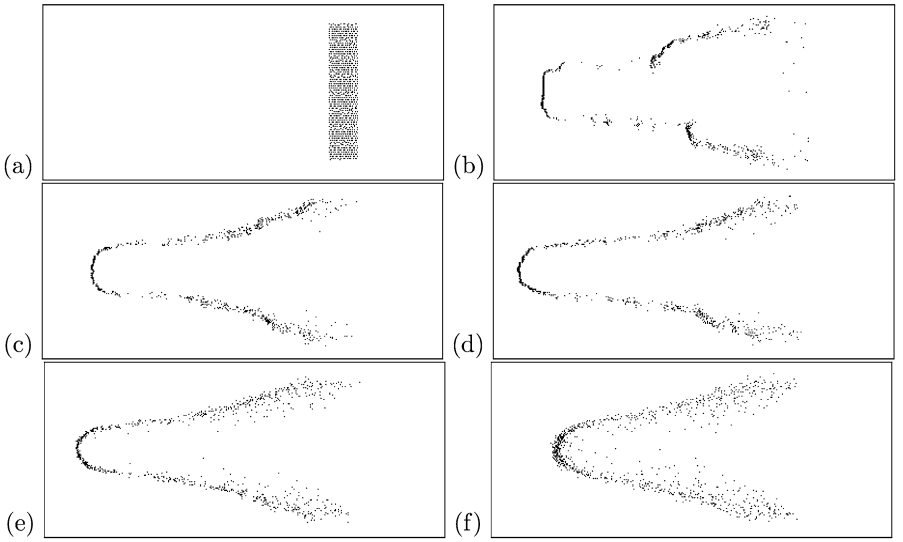

Fig. 15 Example 9. The effect of the medium sensitivity coefficient α_q in the stochastic model. (a) initial configuration. (b) $\alpha_q = 0$ with 750 iterations. (c) $\alpha_q = 0.25$ with 350 iterations. (d) $\alpha_q = 0.5$ with 300 iterations. (e) $\alpha_q = 0.75$ with 250 iterations. (f) $\alpha_q = 1.0$ with 200 iterations.

move α_q^{-1} times slower than if that location has been previously occupied. In particular, when α_q is very close to 1, the medium memory effect is less noticeable. In Fig. 15, we show results obtained with 5,000 bacteria that are initially uniformly distributed in a strip in $\mathbb{R}^2$. The different snapshots correspond to different values of α_q (ranging from 0 to 1). A strong memory effect forces bacteria to move slower into regions that were not previously occupied, which consequently leads to a slow finger formation. The shape of the emerging tip of the finger also depends on the choice of parameters.

Remark 4.2. The only sources of randomness in the model are the Wiener processes $W_i(t)$ and $\tilde{W}_i(t)$ in Eqs. (3) and (4). While the role of the random term in the position process $X_i(t)$ is straightforward, the random term in the definition of $dS_i(t)$ is less noticeable. In fact, the latter has a role only when the configuration of the colony is such that the excitation of the majority of the bacteria is very close to the threshold K. When that happens, the effect of this random term is a very slow motion toward the light source. The reason for such rather slow motion is the fact that bacteria move when their excitation is above the threshold, but do not move when the excitation is less than the threshold level K. Thus, even though the expected value of the random term on the excitation is zero, the expected value of the motion is positive (toward the light source). Notice that to reach such a state the excitation of a considerable number of bacteria must remain close to the threshold K. This can be achieved, e.g., by fixing the initial distribution of cells in $\mathbb{R}^2$ and varying the radius r of the domain of interaction. For a given distribution of cells, the averaged excitation of the colony tends to increase when r increases. Thus, we can manipulate the averaged excitation of the colony by choosing an appropriate value of r.

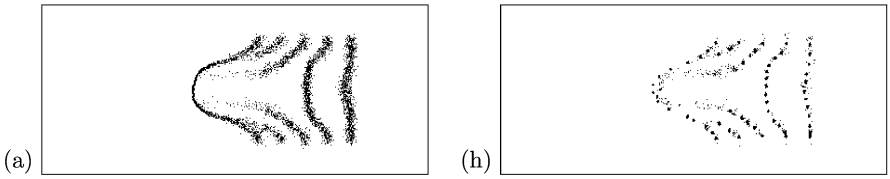

Fig. 16 The role of the density factor v_g in the stochastic model. Shown are $v_g = 0$ (a) and $v_g = 1$ (b). Very high v_g values cause bacteria to aggregate into small clusters, while for smaller values the interfaces are better defined.

Remark 4.3. Another interesting study concerns the effect of the density-dependent term $v_g \nabla \rho^N(t; x, y)$ in Eq. (4). For higher values of v_g, bacteria aggregate in small but very well- defined clusters. For values that are closer to zero, it is possible to distinguish between the interfaces. A comparison with the experimental results from Section 2 suggests that we should consider smaller values of v_g rather than larger. Even the case $v_g = 0$ yields very satisfactory results when comparing with the movie sequences in Section 2. Hence, it is reasonable to remove that term from the model. In fact, the method used for the derivation of the PDE system (6) in Levy and Requeijo (2008) cannot be used if a term that depends on the gradient of the density of bacteria is present. Figure 16 shows the results after 500 iterations for two different values of v_g.

Remark 4.4. We note that Eq. (3) can be replaced by a modified excitation process,

$$\frac{dS_i(t)}{S_i(t)} = a\big(\mu_i(t) - S_i(t)\big)\,dt + \sigma\,dW_i(t). \tag{8}$$

Here, $a\colon \mathbb{R} \to \mathbb{R}$ is a strictly increasing continuous function. Equation (8) allows us to manipulate how fast cells *acquire* or *lose* excitation (by choosing an appropriate response function a). Since $S_i(t)$ tends to move toward the reverting level $\mu_i(t)$, it is possible to control how fast bacteria gain excitation by modifying $a(y)$ for positive values of y (where $y = \mu_i(t) - S_i(t)$). Similarly, we can control how long bacteria remain excited by changing $a(y)$ for negative values of y.

Remark 4.5. One of the main differences between the stochastic model and the cellular automaton model is the mechanism dictating the excitation dynamics. In the CA model, we use a very simple algorithm for controlling the excitation dynamics; the excitation of each cell has a fixed decay rate, and it grows proportionally to the total excitation on its domain of interaction. In the stochastic model, a mean reverting process guides how excitation evolves in time. The mean reverting level is computed by averaging the total excitation on the domain of interaction. Another major difference between both models concerns cell overlapping; in the cellular automaton, only one cell can occupy a grid-point at any given time. The stochastic model, on the other hand, allows multiple cells to occupy the same point in space.

5. Conclusion

In this work, we presented different models to describe the motion patterns that were observed in Synechocystis sp. cells exhibiting phototaxis. In both models, the property of the individual bacterium, which we refer to as *excitation*, propagates to nearby cells, leading to a very complex dynamics. Our models also account for a *surface memory* that facilitates the movement of cells traveling to locations previously occupied.

The excitation mechanism we propose as part of the phototaxis model assumptions is of critical importance. It is imperative that the excitation property is not only directly related to the phototactic response of the individual, but it also depends on the excitation of the surrounding bacteria. This property is what distinguishes our phototaxis models from models of chemotaxis. Without excitation, the setup would be similar to chemotaxis, where light could be modeled, e.g., as a persistent chemical of constant gradient pointing to the light source. This, however, will not explain the delayed initiation of motion toward light. It is also not obvious how fingers with stable boundaries would emerge without taking into account a group-related dynamics.

The dynamics of the excitation process determines the way cells influence surrounding cells, and consequently how the colony reacts to the light sources. In the models from Sections 3.1–3.2, we considered two distinct dynamical models that lead to motion patterns resembling the observations discussed in Section 2. In the CA model, the excitation decays at a constant rate, and increases proportionally to the total excitation of neighboring cells. This excitation dynamics is relevant also in the setting of the PDE system (6), as the functions β and γ represent precisely the creation and depletion of excitation. For the stochastic model in Section 4.2, the dynamics of the excitation process is more complex, pointing at all times towards a weighted average of the total excitation of the neighboring cells.

While there is no equivalent in chemotaxis to the excitation process, the surface memory process L can be viewed as a chemoattractant. In fact, one of our assumptions is that cells can sense the gradient changes of such chemicals and resist moving in the direction of decreasing gradients. The main difference with the chemotaxis setting is that here we assume that this chemical does not decay, that it is not consumed by bacteria, and that it is produced at a very fast rate (up to a certain level). This means that in practice we can then approximate it at all times by either zero or one.

The role that the light plays in our models is in setting the preferred direction of motion. It is possible to add to the models sensitivity to the intensity of the light. This can be done not only in terms of the speed of motion, but also in terms of how light can contribute to the changes in the excitation of the bacteria. We do not incorporate in our models any mechanism that suggests how cells actually "choose" a direction. The molecular components in phototaxis, including the photoreceptor in Synechocystis sp. Strain PCC6803 have been recently identified (see Bhaya, 2004; Bhaya et al., 2001).

The numerical simulations in Section 4.2 clarify the role of the various terms that appear in the stochastic model. By changing the parameters appropriately, we can control the characteristics of this model, such as the shape and speed of fingers, how noticeable the motion momentum effect is, or even the amount of cells left behind when the colony moves toward the light.

Another important conclusion resulting from the numerical simulations concerns the term $v_g \nabla \rho^N$ in (4); the simulations suggest v_g should be very small, or even zero. This is important as the derivation of the phototaxis system in Levy and Requeijo (2008) relies on the nonexistence of the corresponding ∇u.

Finally, we would like to emphasize that from a biophysical point of view, most of the mechanisms that control the motion of Synechocystis sp. Strain PCC6803 remain unknown. It is our hope that the mathematical models developed here and elsewhere, will provide the biologists with new insights that will come into play in the design (and analysis) of new experiments.

Acknowledgements

The work of D. Levy was supported in part by the NSF under Career Grant DMS-0133511. We would like to thank Devaki Bhaya and Matthew Burriesci for providing us with the images and movies and for their guidance.

References

Bhaya, D., 2004. Light matters: phototaxis and signal transduction in unicellular cyanobacteria. Mol. Microbiol. 53, 745–754.

Bhaya, D., Bianco, N.R., Bryant, D., Grossman, A.R., 2000. Type IV Pilus biogenesis and motility in the cyanobacterium Synechocystis sp. PCC6803. Mol. Microbiol. 37, 941–951.

Bhaya, D., Takahashi, A., Grossman, A.R., 2001. Light regulation of Type IV Pilus-dependent motility by chemosensor-like elements in Synechocystis PCC 6803. Proc. Natl. Acad. Sci. USA 98, 7540–7545.

Bhaya, D., Levy, D., Requeijo, T., 2008. Group dynamics of phototaxis: interacting stochastic many-particle systems and their continuum limit. In: Benzoni-Gavage, S., Serre, D. (Eds.), Hyperbolic Problems: Theory, Numerics, Applications, Proceedings of the Eleventh International Conference on Hyperbolic Problems, Lyon, 2006, pp. 145–159. Springer, Berlin.

Black, W.P., Xu, Q., Yang, Z., 2006. Type IV Pili function upstream of the dif chemotaxis pathway in Myxococcus xanthus EPS regulation. Mol. Micobiol. 61, 447–456.

Burriesci, M., Bhaya, D., 2008. Tracking phototactic responses and modeling motility of Synechocystis sp. strain PCC6803. J. Photochem. Photobiol. B, Epub ahead of print.

Childress, S., Levandowsky, M., Spiegel, E., 1975. Pattern formation in a suspension of swimming microorganisms: equations and stability theory. J. Fluid Mech. 69, 591–613.

Keller, E.F., Segel, L.A., 1971. Traveling band of chemotactic bacteria: a theoretical analysis. J. Theor. Biol. 30, 235–248.

Levy, D., Requeijo, T., 2008. Modeling group dynamics of phototaxis: from particle systems to PDEs. Discrete Contin. Dyan. Syst. B 9, 108–128.

Li, Y., Sun, H., Ma, X., Lu, A., Lux, R., Zusman, D., Shi, W., 2003. Extracellular polysaccharides mediate pilus retraction during social motility of Myxococcus xanthus. Proc. Natl. Acad. Sci. USA 100, 5443–5448.

Lu, A., Cho, K., Black, W.P., Duan, X.Y., Lux, R., Yang, Z., Kalan, H.B., Zusman, D.R., Shi, W., 2005. Exopolysaccharide biosynthesis genes required for social motility in Myxococcus xanthus. Mol. Microbiol. 55, 206–220.

Maree, A., Panfilov, A., Hogeweg, P., 1999. Phototaxis during the slug stage of Dictyostelium discoideum: a model study. Proc. R. Soc. Lond. B 266, 1351–1360.

Masuda, S., Ono, T.A., 2004. Biochemical characterization of the major adenylyl cyclase cya 1, in the cyanobacterium Synechocystis sp. PCC 6803. FEBS Lett. 577, 255–258.

Masuda, S., Ono, T.A., 2005. Adenylyl cyclase activity of cya1 from the cyanobacterium Synechocystis sp. strain PCC 6803 is inhibited by bicarbonate. J. Bacteriol. 187, 5032–5035.

Oelschläger, K., 1989. On the derivation of reaction-diffusion equations as limit dynamics of systems of moderately interacting stochastic many-particle processes. Probab. Theory Relat. Fields 82, 565–586.

Ohmori, M., Okamoto, S., 1979. Photomovement of motile microorganisms. Photochem. Photobiol. 29, 423–437.
Stevens, A., 2000a. A stochastic cellular automaton modeling gliding and aggregation of myxobacteria. SIAM J. Appl. Math. 61, 172–182.
Stevens, A., 2000b. The derivation of chemotaxis equations as limit dynamics of moderately interacting stochastic many-particle systems. SIAM J. Appl. Math. 61, 183–212.
Terauchi, K., Ohmori, M., 1999. An adenylate cyclase, cya1, regulates cell motility in the cyanobacterium Synechocystis sp. PCC 6803. Plant Cell Physiol. 40, 248–251.
Yoshimura, H., Yanagisawa, S., Kanehisa, M., Ohmori, M., 2002a. Screening for the target gene of cyanobacterial cAMP receptor protein SYCRP1. Mol. Microbiol. 43, 834–853.
Yoshimura, H., Yoshihara, S., Okamoto, S., Ikeuchi, M., Ohmori, M., 2002b. A cAMP receptor protein, SYCRP1, is responsible for the cell motility of Synechocystic sp. PCC 6803. Plant Cell. Physiol. 43, 460–463.
Youderian, P., Hartzell, P.L., 2006. Transposon insertions of Magellan-4 that impair social gliding motility in Myxococcus xanthus. Genetics 172, 1397–1410.
Yu, R., Kaiser, D., 2007. Gliding motility and polarized slime secretion. Mol. Microbiol. 63, 454–467.